

Thermodynamic and hydrodynamic characteristics of interacting system formed in relativistic heavy ion collisions

Xu-Hong Zhang^{1,*}, Hao-Ning Wang^{2,†}, Fu-Hu Liu^{1,‡}, Khusniddin K. Olimov^{3,4,§}

¹*State Key Laboratory of Quantum Optics and Quantum Optics Devices,
Institute of Theoretical Physics, Shanxi University, Taiyuan 030006, China*

²*College of Mechanical and Vehicle Engineering,
Taiyuan University of Technology, Taiyuan 030024, China*

³*Laboratory of High Energy Physics, Physical-Technical Institute of Uzbekistan Academy of Sciences,
Chingiz Aytmatov Str. 2b, Tashkent 100084, Uzbekistan*

⁴*Department of Natural Sciences, National University of Science and Technology
MISIS (NUST MISIS), Almalyk Branch, Almalyk 110105, Uzbekistan*

Abstract: To study the energy-dependent characteristics of thermodynamic and hydrodynamic parameters, based on the framework of a multi-source thermal model, we analyze the soft transverse momentum (p_T) spectra of the charged particles (π^- , π^+ , K^- , K^+ , \bar{p} , and p) produced in gold–gold (Au–Au) collisions at the center-of-mass energies $\sqrt{s_{NN}} = 7.7, 11.5, 14.5, 19.6, 27, 39, 62.4,$ and 200 GeV from the STAR Collaboration and in lead–lead (Pb–Pb) collisions at $\sqrt{s_{NN}} = 2.76$ and 5.02 TeV from the ALICE Collaboration. In the rest framework of emission source, the probability density function obeyed by meson momenta satisfies the Bose-Einstein distribution, and that obeyed by baryon momenta satisfies the Fermi-Dirac distribution. To simulate the p_T of the charged particles, the kinetic freeze-out temperature T and transverse expansion velocity β_T of emission source are introduced into the relativistic ideal gas model. Our results, based on the Monte Carlo method for numerical calculation, show a good agreement with the experimental data. The excitation functions of thermodynamic parameter T and hydrodynamic parameter β_T are then obtained from the analyses, which shows an increase tendency from 7.7 GeV to 5.02 TeV in collisions with different centralities.

Keywords: Multi-source thermal model, Transverse momentum spectra, Bose-Einstein (Fermi-Dirac) distribution, Thermodynamic and hydrodynamic parameters (characteristics)

PACS: 12.40.Ee, 13.85.Hd, 24.10.Pa

I. INTRODUCTION

The strong interaction, which was used to describe the nuclear force between nucleons (protons or neutrons) at the earliest stage of the universe evolution, is the strongest one [1, 2], being 38 orders of magnitude greater than gravity. As it differs from the atomic and molecular scale interactions, scientists usually use quantum chromodynamics (QCD) to describe the strong interactions

between particles below the size of a nucleus [3–5]. In recent years, the research on “new state of matter”, formed in relativistic heavy ion collisions, has attracted many scientists in the field of high energy physics in the world [6].

In extreme conditions, raising the temperature of the system, or increasing its density, the QCD substance will produce two particular phase transitions, one is the deconfinement phase transition and the other is the chiral phase transition [7, 8]. The former corresponds to the disappearance of quark confinement, meaning that quarks are free to move to other regions of the nuclear matter, not just confined to the movement inside the nucleon. The latter corresponds to the restoration of eigensymmetry, that is, the kinetic mass becomes zero and the quarks become as particles, close to zero-mass, while at

*xhzhang618@163.com; zhang-xuhong@qq.com

†wanghaoning517@139.com

‡Correspondence: fuhuliu@163.com; fuhuliu@sxu.edu.cn

§Correspondence: khkolimov@gmail.com; kh.olimov@uzsci.net

the same time, the existence of phase transitions indicates the emergence of a new state of matter.

Observation of these two phase transitions in a high-temperature dense region implies the transition of a substance to a state with quark-gluons as the fundamental degree of freedom, and this new state of matter is named quark-gluon plasma (QGP) [9–11]. In QGP expansion, a lot of particles are produced, and finally they are measured in experiments. One may study the formation and change of the new state of matter from the dynamic evolution of the final state particles. Such a matter is usually described by QCD phase diagram [7, 8], and the thermodynamic properties of the system are expressed by the temperature and the chemical potential of the baryons.

When the system undergoes phase transition and reaches the equilibrium state of chemical and kinetic freeze-out stage, the thermodynamic properties of the final state particles can be studied, which is of great significance to obtain the critical point of phase transition and understand the characteristics of QCD. In addition, under low temperature and high density condition, QCD substance will form color superconducting state [12–14] through phase transition. The above two new states of matter do not exist stably, and the heavy ion colliders can be used to control the system state, which provides a powerful tool for researchers to study the QCD phase transition.

As an open question, the energy of the critical point is worth studying by various ways [15–19]. One of them is to study the energy-dependent relations or the excitation functions of different parameters which include, but are not limited to, the thermodynamic parameter T and the hydrodynamic parameter β_T . Generally, an inflection point or sudden change in the excitation functions implies the existence of critical point or a change of interaction mechanism. Experiments in relativistic heavy ion collisions [20, 21] have provided a new chance for ones to explore new matter and phenomena under extreme conditions. Meanwhile, one may test different theories or models and explain the new effects [22–24].

The whole process of relativistic heavy ion collisions can be divided into three stages: pre-equilibrium dynamics, viscous fluid dynamics, and free flow. In the collisions, a large number of particles are generated and escaped. At the last stage of free flow (i.e. the stage of kinetic freeze-out), one is curious whether the widely used relativistic ideal gas model [25–27] can be applied. If yes, escaped fermions should be subject to Fermi-Dirac statistics and bosons follow the Bose-Einstein statistics. This can be done if one assumes that the generated parti-

cles come from the equilibrium stationary source, though the evolution process is represented by a perfect liquid.

However, because the process of relativistic heavy ion collisions is very complex and the number of produced particles is very large. It is possible that an equilibrium stationary source is not enough to describe more characteristics. One naturally thinks of a multi-source scenario, the multi-source thermal model [28, 29], which assumes multiple equilibrium stationary sources, and there are interactions among these sources. Due to the extreme squeeze between projectile and target nuclei, a transverse expansion of the interacting system (emission source) or a transverse flow of the final state particles will appear, which affects particle momentum and related quantities in experimental spectra. One is also curious whether the multi-source thermal model describes appropriately the transverse flow.

In this paper, starting from the probability density function of momenta in the relativistic form, we perform numerical calculations in two steps to analyze the soft transverse momentum (p_T) spectra of the final state particles generated in high energy gold-gold (Au–Au) and lead-lead (Pb–Pb) collisions measured by the STAR [30–34] and ALICE Collaborations [35, 36], respectively. The thermodynamic parameter T (kinetic freeze-out temperature) and the hydrodynamic parameter β_T (transverse expansion velocity) of the interacting system (emission source) are extracted. In the first step, in the rest frame of emission source, using a parameter T [37–40], the momentum and its each component and energy are sampled according to the assumption of anisotropic emission and a given momentum distribution. In the second step, a new transverse momentum distribution is obtained according to the Lorentz transformation [41] at a given β_T [41–45].

The remainder of this paper is structured as follows. Section 2 introduces the related theoretical distribution and methods of calculations. The comparison and discussion of the results are presented in Section 3. Finally, in Section 4, we summarize and list our main observations and conclusions.

II. FORMALISM AND METHOD

According to the multi-source thermal model [28, 29], many emission sources are assumed to form in high energy collisions. Each stationary emission source emits isotropically particles in various directions. Furthermore, at the kinetic freeze-out, we consider the relativistic ideal gas model [25–27] for the escaped particles in the sta-

tionary source. The momentum (p') distribution of the emitted particles obeys the standard distribution [27, 46],

$$f(p') = \frac{1}{N} \frac{dN}{dp'} = Cp'^2 \left[\exp \left(\frac{\sqrt{p'^2 + m_0^2} - \mu}{T} \right) + S \right]^{-1} \quad (1)$$

which is the probability density function. Here, N is the number of particles, $C = (1/m_0^2 kT)[1/K_2(m_0/kT)]$ is the normalization constant, $K_2(m_0/kT)$ is the modified second-order Bessel function correction, $k = 1$ is the Boltzmann constant in the system of natural units, T is the temperature of the emission source, and m_0 and μ are the rest mass and chemical potential of the particle, respectively. When $S = +1, 0$, and -1 , the function corresponds to the Fermi-Dirac distribution, Boltzmann distribution, and Bose-Einstein distribution, respectively [47].

Generally, if $m_0 \gg \mu$, the quantum effect plays a small role, so we can ignore the influence of the chemical potential when studying the momentum distribution in collisions at higher energy. In case of $m_0 \approx \mu$, the role of the chemical potential increases significantly, and it is necessary for us to distinguish the fermions and bosons. For the case of $m_0 \ll \mu$, the absolute value, $|\sqrt{p'^2 + m_0^2} - \mu|$, should be used to avoid $\sqrt{p'^2 + m_0^2} - \mu < 0$ in low- p' region. In fact, μ is small enough in this work and the case of $\sqrt{p'^2 + m_0^2} - \mu < 0$ does not exist. Although we may regard μ as a free parameter, its value can be obtained in different ways.

Empirically, for baryons, the chemical potential μ_B is given by [48–51],

$$\mu_B = \frac{1.303}{1 + 0.286\sqrt{s_{NN}}}, \quad (2)$$

where $\sqrt{s_{NN}}$ is the collision energy (center-of-mass energy) per nucleon pair, and both μ_B and $\sqrt{s_{NN}}$ are in GeV. Approximately, the chemical potential μ_p of the proton is given by μ_B , and the chemical potential μ_π (μ_K) of the pion (kaon) is taken from a method based on the yield ratio of negative to positive particles [34].

For the convenience of subsequent calculations, we use the Monte Carlo method [5, 52, 53] to obtain the momentum distribution and discrete values of each component and energy. Let $R_{1,2,3}$ be random numbers that follow a uniform distribution in the range of $[0, 1]$. For a discrete p' , it satisfies the momentum sampling:

$$\int_0^{p'} f(p'') dp'' < R_1 < \int_0^{p'+\delta p'} f(p'') dp'', \quad (3)$$

where $\delta p'$ is a small shift from p' and $f(p'')$ is just Eq. (1). The azimuthal angle of the isotropic emission is obtained by

$$\varphi' = 2\pi R_2, \quad (4)$$

and the emission angle is

$$\vartheta' = 2 \arcsin \sqrt{R_3}. \quad (5)$$

Thus, in the rectangular coordinate system $O-xyz$, where Oz axis is the beam direction and xOz plane is the reaction plane, one obtains the x -component of the momentum,

$$p'_x = p' \sin \vartheta' \cos \varphi', \quad (6)$$

and the y -component of the momentum,

$$p'_y = p' \sin \vartheta' \sin \varphi', \quad (7)$$

the transverse momentum,

$$p'_T = p' \sin \vartheta', \quad (8)$$

the z -component of the momentum,

$$p'_z = p' \cos \vartheta', \quad (9)$$

and the energy,

$$E' = \sqrt{p'^2 + m_0^2}. \quad (10)$$

Now we consider the Lorentz transformation from the stationary source to the expanding one, which is caused by the interactions among multiple sources. Let $\beta_{x,y,z}$ denote the components of the expansion velocity. We have

$$p_x = \frac{1}{\sqrt{1 - \beta_x^2}} (p'_x + \beta_x E'), \quad (11)$$

$$p_y = \frac{1}{\sqrt{1 - \beta_y^2}} (p'_y + \beta_y E'), \quad (12)$$

and

$$p_z = \frac{1}{\sqrt{1 - \beta_z^2}} (p'_z + \beta_z E'). \quad (13)$$

The transverse momentum is given by

$$p_T = \sqrt{p_x^2 + p_y^2} = \frac{1}{\sqrt{(1 - \beta_x^2)(1 - \beta_y^2)}} \times \sqrt{(1 - \beta_y^2)(p'_x + \beta_x E')^2 + (1 - \beta_x^2)(p'_y + \beta_y E')^2}. \quad (14)$$

Here, $\sqrt{\beta_x^2 + \beta_y^2} = \beta_T$. Due to the small difference between β_x and β_y , we ignore this difference and take $\beta_x = \beta_y$ for simplicity when describing the transverse momentum spectrum. It should be noted that the difference cannot be ignored in analyzing anisotropic flow.

It should be noted that Eq. (13) contains only the proper expansion, but not the longitudinal expansion or motion of the emission source. If the longitudinal effect is considered, we may use a larger β_z in Eq. (13). In this case, the ‘‘expansion’’ of emission source is anisotropic in the three dimensional momentum space, though the expansion can be taken to be isotropic in the transverse plane when the transverse anisotropic flow is not the topic of the present work.

In the transverse plane, if the interactions among various sources are considered, an anisotropic flow will be observed. Although one may use $\beta_x \neq \beta_y$ to describe the transverse anisotropic flow, which results in anisotropic p_x and p_y distributions, we may also have an alternative method. In our previous work [54], to extract the property of transverse anisotropic flow, one may appropriately revise Eqs. (11) and (12) to be

$$p_x = \frac{a_x}{\sqrt{1 - \beta_x^2}}(p'_x + \beta_x E') + b_x \quad (15)$$

and

$$p_y = \frac{a_y}{\sqrt{1 - \beta_y^2}}(p'_y + \beta_y E') + b_y \quad (16)$$

respectively. Here, the parameters a_x and b_x (a_y and b_y) describe the source’s expansion and displacement along Ox (Oy) axis respectively.

Generally, $a_{x,y} = 1$ and $b_{x,y} = 0$ imply an isotropic source. For an anisotropic source, $a_{x,y} > 1$ describes an expansion, and $b_{x,y} > 0$ ($b_{x,y} < 0$) describes a displacement along the positive (negative) direction [54]. Although $a_{x,y} < 1$ may describe a contraction in mathematics, the physics condition gives $a_{x,y} \geq 1$ in the expansion stage of the system. One may use the elliptic flow

$$v_2 = \langle \cos(2\varphi) \rangle = \left\langle \frac{p_x^2 - p_y^2}{p_x^2 + p_y^2} \right\rangle \quad (17)$$

to describe the strength of the transverse anisotropic flow, where $\langle \dots \rangle$ denotes an average over the considered data sample. Comparing with β_T , the influence of v_2 on p_T spectra is very small, which can be neglected in the following analyses.

We would like to point out that, as a data-driven work, the current analysis does not model any viscous

hydrodynamics approach. Instead, one may use the p_T spectra to extract some temperatures to describe the excitation degrees of the system at the related stages, where the temperatures are free parameters. In fact, the kinetic freeze-out temperature T and transverse expansion velocity β_T of emission source used in this study are set as free parameters. They describe the thermodynamic and hydrodynamic characteristics of the interacting system at the stage of kinetic freeze-out respectively.

III. RESULTS AND DISCUSSION

A. Comparison with data

To search for the energy of expected critical point of hadronic matter transition to QGP, we may consider to study the energy-dependent characteristics of thermodynamic and hydrodynamic parameters, i.e. the excitation functions of these parameters. This means that we have to collect and fit a large number of data and display them in lots of figures. In fact, incomplete data cannot give a whole excitation function, and the information extracted from the incomplete excitation function may be misleading. In the case of using lots of data and to make the structure of this paper compact, we try to draw the same kind of data in a figure.

Transverse momentum spectra of the final state particles generated in Au–Au and Pb–Pb collisions over an energy range from 7.7 GeV to 5.02 TeV, measured by the STAR [30–34] and ALICE [35, 36] Collaborations, and then performed a fitting analysis on them are displayed in Figures 1–3. In order to compare the properties of the p_T spectra at all energies more comprehensively, we limit the range of p_T to be equal to or less than 3 GeV/ c , which falls into the soft p_T region. Concretely, in the fit, the spectra in the range of $0.2 < p_T < 2.5$ GeV/ c is used to exclude the contributions of resonance decay and hard scattering process [32–34] as much as possible. Different symbols represent the experimental data in different centrality classes, and the curves are our results calculated by the Monte Carlo method. In addition, for showing p_T spectra more clearly in different centrality classes, we indented the data to the power of 10 (such as the numbers in parentheses in the legend). The length of the gray rectangle in the figure represents the error of p_T , and the width represents the error of p_T spectrum $[(1/2\pi p_T)d^2N/dydp_T]$, which is the quadratic sum of the statistical and systematic uncertainties.

Figure 1 shows the result of fitting analysis of p_T spec-

tra of negatively and positively charged pions (π^- and π^+) from central (0–5% or 0–10%) to peripheral (70–80% or 40–80%) collisions using the Bose-Einstein distribution embedded an expansion velocity. Panels (a)–(j) represent the p_T spectra at different collision energies shown in the figure. The closed (open) symbols and solid (dashed) curves correspond to π^- (π^+), and there is no distinction between π^- and π^+ in panel (j). The experimental data presented in panels (a)–(h) are quoted from the STAR Collaboration for Au–Au collisions, which shows the mid-rapidity range of $|y| < 0.1$ [30–34]; and the experimental data presented in panels (i) and (j) are collected from ALICE Collaboration for Pb–Pb collisions, whose mid-(pseudo)rapidity range is $|y| < 0.5$ [35] and $|\eta| < 0.8$ [36]. The values of the free parameters T and β_T extracted from the fits will be analyzed in next subsection. Following each panel, the ratios of Data/Fit are given to show the quality of the fit.

Similar to Figure 1, Figures 2 and 3 show the p_T spectra of negative and positive kaons (K^- , K^+ , or $K^- + K^+$) and anti-protons and protons (\bar{p} , p , or $\bar{p} + p$) respectively [30–36], where the spectra in Figure 2 are fitted with the Bose-Einstein distribution with embedded transverse expansion velocity and the spectra in Figure 3 are fitted with the Fermi-Dirac distribution with embedded transverse expansion velocity. The related parameters will be analyzed in next subsection.

From Figures 1–3 one can see that the Bose-Einstein/Fermi-Dirac distribution with embedded transverse expansion velocity can describe the soft p_T spectra of light charged particles produced in high-energy Au–Au and Pb–Pb collisions at the Relativistic Heavy Ion Collider and the Large Hadron Collider. In the description, there are only two free parameters: the kinetic freeze-out temperature T and the transverse expansion velocity β_T . Compared with the general treatments in the community, the present work has used a more clear picture and a simpler distribution. In fact, the Bose-Einstein/Fermi-Dirac distribution is the most basic one in the ideal gas model.

From the ratios of Data/Fit, one can see that in very low p_T region and around $p_T \approx 3$ GeV/ c , the fitting results underestimate the data in some cases. This means that we need a very soft component for the contribution of resonance decay. Meanwhile, we need a hard component for the contribution of hard scattering process. Naturally, a multi-component distribution can be applied for the whole p_T region. Generally, for the extraction of thermodynamic and hydrodynamic characteristics of interacting system, the contributions of reso-

nance decay and hard process to the p_T spectra should be removed because the two contributions come from non-thermal production and undergo non-expansion process. Although other methods can describe the p_T spectra, the present work provides an alternative method in the description. It does have clear picture and methodological significance.

B. Tendencies of parameters

To show the excitation functions of related parameters and extract the variation tendencies of the functions, we analyze the energy-dependent relations of related parameters for different centralities and particles in this subsection. The excitation functions are related to the search for the energy of expected critical point and the change of interaction mechanism, which shows remarkable scientific significance. In addition, we have used a method closer to the relativistic ideal gas model [25–27] than the blast-wave model [31, 35, 42] in fitting the transverse momentum spectra. It is also interesting to compare the results of two fittings.

Figure 4 shows the dependence of T on the collision energy $\sqrt{s_{NN}}$, centrality class (percentage), and particle mass. From panels (a) to (i), the centrality classes are 0–5%, 5–10%, ..., 70–80%, respectively. The centrality classes at 62.4 and 200 GeV are different in some cases which shows in the panels. The closed (open) squares, circles, and triangles represent the results for π^- (π^+), K^- (K^+), and \bar{p} (p), respectively. The weighted averages over the yields of different particles are shown by the crosses. One can see that T increases generally with some fluctuations as the increase of collision energy. From central to peripheral collisions, T has a slight decrease. In central collisions, T increases with the increase of particle mass, and in peripheral collisions the situation seems to be different or ambiguous. The dependence of T on isospin is not significant.

Figure 5 is similar to Figure 4, but it shows the dependence of β_T on the collision energy, centrality class, and particle mass. One can see that β_T increases generally with some fluctuations as the increase of collision energy. From central to peripheral collisions, β_T has a slight decrease. In central collisions, β_T does not change significantly with the increase of particle mass, and in peripheral collisions, β_T decreases with the increase of particle mass. The dependence of β_T on isospin is also not significant. Compared with T , β_T shows larger fluctuations in the spectra, which is reflected by its errors.

It should be noted that the dependence of T on centrality is an open question at present, though β_T increases with the increase of centrality. Based on the blast-wave model [42], the STAR [30, 31] and ALICE [35] Collaborations shows that T decreases slightly with the increase of centrality. However, our results show that T increases slightly with the increase of centrality. The difference is caused by different methods which also lead to different values in parameters. In the blast-wave model [42], a self-similar and variant flow profile function is used. In the present work, we have used an invariant flow velocity embedded in the relativistic ideal gas model [25–27] for the little bang process of relativistic collisions, which is meaningful in methodology.

In central collisions, although a lower temperature can be explained by a longer lifetime of the system, a higher temperature can be explained by a higher excitation degree. The result of the blast-wave model fitted by the STAR Collaboration [31] shows that T is almost the same in the energy range from 7.7 to 39 GeV and it is lower at 62.4 and 200 GeV. Our result shows that T increases generally from 7.7 GeV to 5.02 TeV. Although the results of both the fittings can be explained by us, it is hard to determine which one is correct. In our opinion, more model work is needed in the future for the complex process of relativistic collisions.

C. Further discussions

Generally, the interacting system of relativistic heavy ion collisions [20, 21] will experience two stages of freeze-out, one is chemical freeze-out and the other is kinetic freeze-out. The two kinds of freeze-outs possibly occur simultaneously or non-simultaneously. It depends on the sizes of chemical and kinetic freeze-out temperatures. In fact, the system is suddenly frozen [55, 56] and the short-lived resonances decay [57], changing the kinetic spectra of stable particles. The resonances of the system, generated during chemical freeze-out, decay rapidly, but the system continues to evolve with elastic collisions between hadrons, and the system will stay in the local thermal equilibrium before kinetic freeze-out [58]. The particles' transverse momentum spectra carry information about it.

If the chemical and kinetic freeze-out temperatures are nearly the same, one may consider that the two freeze-outs occur almost simultaneously. If the two freeze-outs occur at different time moments, the chemical freeze-out happens generally earlier than the kinetic

freeze-out, and the chemical freeze-out temperature is larger than the kinetic one. The temperature T extracted from the present work is only the kinetic freeze-out temperature. The chemical freeze-out temperature is not available here, and we cannot give a comparison for the two temperatures corresponding to the two freeze-outs.

Studying the transverse momentum (mass) spectra of the final state particles, produced in relativistic heavy ion collisions, is an effective and fast means to obtain thermodynamic parameters of the system. The emission source determines the transverse momentum spectra of different kinds of particles. When the interacting system is in the stage of kinetic freeze-out, the emitted particles not only contain thermal motion, but also are affected by the expansion of the system or the flow velocity of the particles. Thermal motion reflects the transverse excitation degree of the system, which can be reflected by the kinetic freeze-out temperature T . The expansion or flow effect embodies the hydrodynamic feature of the system, which can be represented by the transverse expansion or flow velocity β_T .

In the community, the transverse momentum spectra have been studied extensively for different final state particles. The functions usually used in fitting the transverse momentum spectra include the Tsallis distribution [59–61], the Erlang distribution [62–64], the Hagedorn function [65, 66], etc. In the present work, we have adopted the most basic function, the Bose-Einstein/Fermi-Dirac distribution, in the relativistic ideal gas model and introduced the transverse expansion velocity of the system to analyze and fit the transverse momentum spectra of the charged particles, π^- , π^+ , K^- , K^+ , \bar{p} , and p produced in Au–Au and Pb–Pb collisions at high energies, and obtain the thermodynamic parameter T and the hydrodynamic parameter β_T .

Our work shows that the excitation functions of T and β_T increase with the increase of collision energy in the concerned range from 7.7 GeV to 5.02 TeV. This implies that the excitation and expansion degrees of the interacting system are higher at higher energy. The interaction mechanism in the concerned energy range should be the same, which involves the formation of hot dense matter. There is no obvious evidence for the energy of critical point being observed from this work. The energy of expected critical point of hadronic matter transition to QGP is possibly in the lower energy range. Because the most basic function, the Bose-Einstein/Fermi-Dirac distribution, in the relativistic ideal gas model is used, and the transverse expansion velocity of the system is introduced, we consider that the present work has a more

solid foundation than the other distributions or functions used in the community. Moreover, there are only two free parameters in the description of transverse momentum spectra, which is also an advantage of the present work.

It should be noted that the present work shows different tendencies of parameters on collision energy and centrality from the blast-wave model [42] used by the STAR and ALICE Collaborations [30, 31, 35]. The reason is that different pictures and p_T ranges are used in the two methods. Except for the invariant β_T used in the present work and variant β_T used in the STAR and ALICE Collaborations, the present work uses the data in a wider p_T range available in experiments and the STAR and ALICE Collaborations used the data in narrow intermediate- p_T range. For example, the STAR Collaboration pointed out that “the fit ranges used for pions, kaons, and protons are 0.5–1.35 GeV/ c , 0.3–1.35 GeV/ c , and 0.5–1.25 GeV/ c , respectively”, for central Au–Au collisions at 14.5 GeV [31].

Indeed, as mentioned by the STAR and ALICE Collaborations [31, 35], “the blast-wave model fits are very sensitive to the p_T range used”. However, this is not the case of the present work. Although the resonance decays contribute in low- p_T range and the hard scattering process contributes mainly in high- p_T range, it is hard to separate various ranges completely. In fact, the soft thermal process has also large probability to contribute in low- p_T range and small probability to contribute in high- p_T range. In a wider p_T range, the proportion of low- p_T is very large, though that of high- p_T range is very small.

In our opinion, we should use the p_T range as wide as possible in the extraction of kinetic freeze-out parameters from the spectra of soft process. This means that we have to give a consideration to exclude the contributions of resonance decay and hard process to the p_T spectra. However, the boundary in the spectra of different processes is not completely separate. After weighing the pros and cons [32–34], we take $p_T = 0.2\text{--}2.5$ GeV/ c in this work.

Before summary and conclusions, we would like to point out that the equation of state effects (for the interacting medium) on the p_T spectra are not considered into the analysis. The reason is that the assumption of isotropic stationary emission source is applicable, which implies a small influence of the mentioned effects. However, if one studies the anisotropic elliptic flow, the interactions among various sources should be considered. This means that the density of the interacting medium is varying, and then the pressure, temperature, viscosity, and other quantities are changeable in different local re-

gions. These changes are partly reflected by anisotropic elliptic flow which can be described by $a_{x,y}$ and $b_{x,y}$, or different β_x and β_y , in the multi-source thermal model appropriately.

IV. SUMMARY AND CONCLUSIONS

Based on the framework of a multi-source thermal model, we have analyzed the soft transverse momentum spectra of π^- , π^+ , K^- , K^+ , \bar{p} , and p produced in Au–Au collisions at $\sqrt{s_{NN}} = 7.7, 11.5, 14.5, 19.6, 27, 39, 62.4,$ and 200 GeV, measured by the STAR Collaboration, and in Pb–Pb collisions at $\sqrt{s_{NN}} = 2.76$ and 5.02 TeV, measured by the ALICE Collaboration. In the rest framework of emission source, the probability density function of meson momenta satisfies the Bose-Einstein distribution, and that of baryon momenta satisfies the Fermi-Dirac distribution.

Considering the interactions among multiple sources, the emission source has an expansion velocity or the particles have a flow velocity. To simulate the transverse momentum spectra, the kinetic freeze-out temperature and transverse expansion velocity of emission source are introduced. The numerical results, calculated by the Monte Carlo method, are in good agreement with the experimental data of the STAR and ALICE Collaborations. The excitation function, and the centrality and particle mass dependences of kinetic freeze-out temperature and transverse expansion velocity are obtained from the analyses. Being the most basic function, the Bose-Einstein/Fermi-Dirac distribution with the introduced transverse expansion velocity implies that the present work has a solid foundation.

This work does not support the current view that the kinetic freeze-out temperature decreases with the increase of collision energy in the considered energy range. In fact, our work shows that the kinetic freeze-out temperature and the transverse expansion velocity increase generally with the increase of collision energy. The excitation functions of the two parameters do not show a particular structure. This implies that the interaction mechanism in the concerned energy range is the same, though the degrees of excitation and expansion of the system are higher at higher energy. The same mechanism involves the formation of hot dense matter. If existing, the energy of expected critical point of hadronic matter transition to quark-gluon plasma is below the present energy range.

This work also does not support the current view that

the kinetic freeze-out temperature in peripheral collisions is higher than that in central collisions. On the contrary, our work shows that with the increase of centrality from peripheral to central collisions, both the kinetic freeze-out temperature and the transverse expansion velocity have a slight increase. This implies that the degrees of excitation and expansion of the system in central collisions are higher. The reason is that more energy are deposited in central collisions due to the involvement of multiple nucleons.

In addition to energy and centrality dependences, with the increase of particle mass, the kinetic freeze-out temperature increases and the transverse expansion velocity decreases in some cases. This reflects the characteristics of the evolution of hydrodynamic system, in which massive particles are leaved in the early stage at high temperature.

When looking forward into the future, in order to search for the critical point of deconfinement phase transition from hadronic matter to QGP, it is very necessary to study the process of high energy collisions

in lower energy region. The several ongoing heavy ion experiments at a few GeV performed around the world will answer this issue. We look forward to the new results.

Acknowledgments

The work of X.-H.Z. was supported by the Innovative Foundation for Graduate Education in Shanxi University. The work of Shanxi Group was supported by the National Natural Science Foundation of China under Grant No. 12147215, the Shanxi Provincial Natural Science Foundation under Grant No. 202103021224036, and the Fund for Shanxi “1331 Project” Key Subjects Construction. The work of K.K.O. was supported by the Agency of Innovative Development under the Ministry of Higher Education, Science and Innovations of the Republic of Uzbekistan within the fundamental project No. F3-20200929146 on analysis of open data on heavy-ion collisions at RHIC and LHC.

-
- [1] Z. W. Lin and M. Gyulassy, *Phys. Rev. C* **51** (1995) 2177–2187.
- [2] M. Cacciari, P. Nason and R. Vogt, *Phys. Rev. Lett.* **95** (2005) 122001.
- [3] D. Kharzeev and K. Tuchin, *J. High Energy Phys.* **2008**(No. 09) (2008) 093.
- [4] F. Karsch, D. Kharzeev and K. Tuchin, *Phys. Lett. B* **663** (2008) 217–221.
- [5] C. P. Robert and G. Casella, *Monte Carlo Statistical Methods* (Springer Press, New York, USA, 2004), 2nd edition.
- [6] C. Shen, Z. Qiu, H.-C. Song, J. Bernhard and S. Bass *Comp. Phys. Commun.* **199** (2016) 61–85.
- [7] B. Mohanty, *New J. Phys.* **13** (2011) 065031.
- [8] P. Braun-Munzinger and J. Wambach, *Rev. Mod. Phys.* **2009** (2009) 1031–1050.
- [9] H. Satz and R. Stock, *Nucl. Phys. A* **956** (2016) 898–901.
- [10] B. Liu, M. Di Toro, G. Y. Shao, V. Greco, C. W. Shen and Z. H. Li, *Eur. Phys. J. A* **47** (2011) 104.
- [11] H. Bohr and H. B. Nielsen, *Nucl. Phys. B* **128** (1977) 275–293.
- [12] M. Alford, J. A. Bowers and K. Rajagopal, *Phys. Rev. D* **63** (2001) 074016.
- [13] M. Huang and I. A. Shovkovy, *Phys. Rev. D* **70** (2004) 094030.
- [14] P. F. Bedaque, H. Caldas and G. Rupak, *Phys. Rev. Lett.* **91** (2003) 247002.
- [15] X. F. Luo for the STAR Collaboration, *Nucl. Phys. A* **904–905** (2013) 911c–914c.
- [16] P. Tribedy for the STAR Collaboration, *Nucl. Phys. A* **904–905** (2013) 463c–466c.
- [17] N. R. Sahoo for the STAR Collaboration, *J. Phys.: Conf. Ser.* **535** (2014) 012007.
- [18] STAR Collab. (M. S. Abdallah *et al.*), *Phys. Rev. Lett.* **128** (2022) 202303.
- [19] Z. B. Tang, Y. C. Xu, L. J. Ruan, G. V. Buren, F. Q. Wang, and Z. B. Xu, *Phys. Rev. C* **79** (2009) 051901(R).
- [20] PHENIX Collab. (K. Adcox *et al.*), *Nucl. Phys. A* **757** (2005) 184–283.
- [21] STAR Collab. (J. Adams *et al.*), *Nucl. Phys. A* **757** (2005) 102–183.
- [22] N. Xu (for the STAR Collaboration) *Nucl. Phys. A* **931** (2014) 1–12.
- [23] A. Andronic, P. Braun-Munzinger, K. Redlich and J. Stachel, *Nature* **561** (2018) 321–330.
- [24] S. Gupta, X.-F. Luo, B. Mohanty, H. G. Ritter and N. Xu, *Science* **332** (2011) 1525–1528.
- [25] J. Cleymans and D. Worku, *Eur. Phys. J. A* **48** (2012) 160.
- [26] P. N. Pandita, *Phys. Rev. E* **89** (2014) 032110.
- [27] C. D. Dermer, *Astrophys. J.* **280** (1984) 328–333.
- [28] F.-H. Liu, N. N. Abd Allah and B. K. Singh, *Phys. Rev.*

- C* **69** (2004) 057601.
- [29] F.-H. Liu, C.-X. Tian, M.-Y. Duan and B.-C. Li, *Adv. High Energy Phys.* **2012** (2012) 287521.
- [30] STAR Collab. (L. Adamczyk *et al.*), *Phys. Rev. C* **96** (2017) 044904.
- [31] STAR Collab. (J. Adam *et al.*), *Phys. Rev. C* **101** (2020) 024905.
- [32] STAR Collab. (B. I. Abelev *et al.*), *Phys. Rev. C* **79** (2009) 034909.
- [33] STAR Collab. (B. I. Abelev *et al.*), *Phys. Lett. B* **655** (2007) 104–113.
- [34] PHENIX Collab. (S. S. Adler *et al.*), *Phys. Rev. C* **69** (2004) 034909.
- [35] ALICE Collab. (B. Abelev *et al.*), *Phys. Rev. C* **88** (2013) 044910.
- [36] ALICE Collab. (S. Acharya *et al.*), *Phys. Rev. C* **101** (2020) 044907.
- [37] G. Wilk and Z. Włodarczyk, *Eur. Phys. J. A* **48** (2012) 161.
- [38] T. S. Biró, G. G. Barnaföldi, G. Birö and K. M. Shen, *J. Phys.: Conf. Ser.* **779** (2017) 012081.
- [39] G. Wilk and Z. Włodarczyk, *Phys. Rev. Lett.* **84** (2000) 2770.
- [40] T. S. Biró, P. Ván, G. G. Barnaföldi and K. Ürmösy, *Entropy* **16** (2104) 6497–6514.
- [41] H. Niemi, K. J. Eskola and R. Paatelainen, *Phys. Rev. C* **93** (2016) 024907.
- [42] E. Schnedermann, J. Sollfrank and U. Heinz, *Phys. Rev. C* **48** (1993) 2462–2475.
- [43] M. Waqas and B.-C. Li, *Adv. High Energy Phys.* **2020** (2020) 1787183.
- [44] K. J. Eskola, H. Niemi and R. Paatelainen, *Nucl. Part. Phys. Proc.* **276–278** (2016) 161–164.
- [45] F.-H. Liu and H.-L. Lao, *Indian J. Phys.* **90** (2016) 1077–1085.
- [46] C. R. Meng, *Chin. Phys. Lett.* **26** (2009) 102501.
- [47] P. Z. Ning, L. Li and D. F. Min, *Foundation of Nuclear Physics: Nucleons and Nuclei* (Higher Education Press, Beijing, China, 2003).
- [48] A. Andronic, P. Braum-Munzinger and J. Stachel, *Nucl. Phys. A* **834** (2010) 237c–240c.
- [49] A. Andronic, P. Braum-Munzinger and J. Stachel, *Nucl. Phys. A* **772** (2006) 167–199.
- [50] A. Andronic, P. Braum-Munzinger and J. Stachel, *Acta Phys. Pol. B* **40** (2009) 1005–1012.
- [51] J. Cleymans, H. Oeschler, K. Redlich and S. Wheaton, *Phys. Rev. C* **73** (2006) 034905.
- [52] N. Metropolis and S. Ulam, *J. Am. Stat. Assoc.* **44** (1949) 335–341.
- [53] D. E. Raeside, *Phys. Med. Biol.* **21** (1976) 181–197.
- [54] F.-H. Liu, J.-S. Li, M.-Y. Duan, *Phys. Rev. C* **75** (2007) 054613.
- [55] W. Broniowski and W. Florkowski, *Phys. Rev. Lett.* **87** (2001) 272302.
- [56] A. Motornenko, V. Vovchenko, C. Greiner and H. Stoecker, *Phys. Rev. C* **102** (2020) 024909.
- [57] A. Mazeliauskas and V. Viskavicius, *Phys. Rev. C* **101** (2020) 014910.
- [58] J. Chen, J. Deng, Z. B. Tang, Z. B. Xu and L. Yi, *Phys. Rev. C* **104** (2021) 034901.
- [59] H. Zheng and L. L. Zhu, *Adv. High Energy Phys.* **2015** (2020) 180491.
- [60] H. Zheng, L. L. Zhu and A. Bonasera, *Phys. Rev. D* **92** (2015) 074009.
- [61] CMS Collab. (S. Charchyan *et al.*), *Eur. Phys. J. C* **72** (2012) 2164.
- [62] F.-H. Liu and J.-S. Li, *Phys. Rev. C* **78** (2008) 044602.
- [63] F.-H. Liu, *Nucl. Phys. A* **810** (2008) 159–172.
- [64] F.-H. Liu, Y.-Q. Gao, T. Tian and B.-C. Li, *Eur. Phys. J. A* **50** (2014) 94.
- [65] ALICE Collab. (B. Abelev *et al.*), *Eur. Phys. J. C* **75** (2015) 1.
- [66] H. Hagedorn, *Riv. Nuovo Cim.* **6**(No. 10) (1983) 1–50.

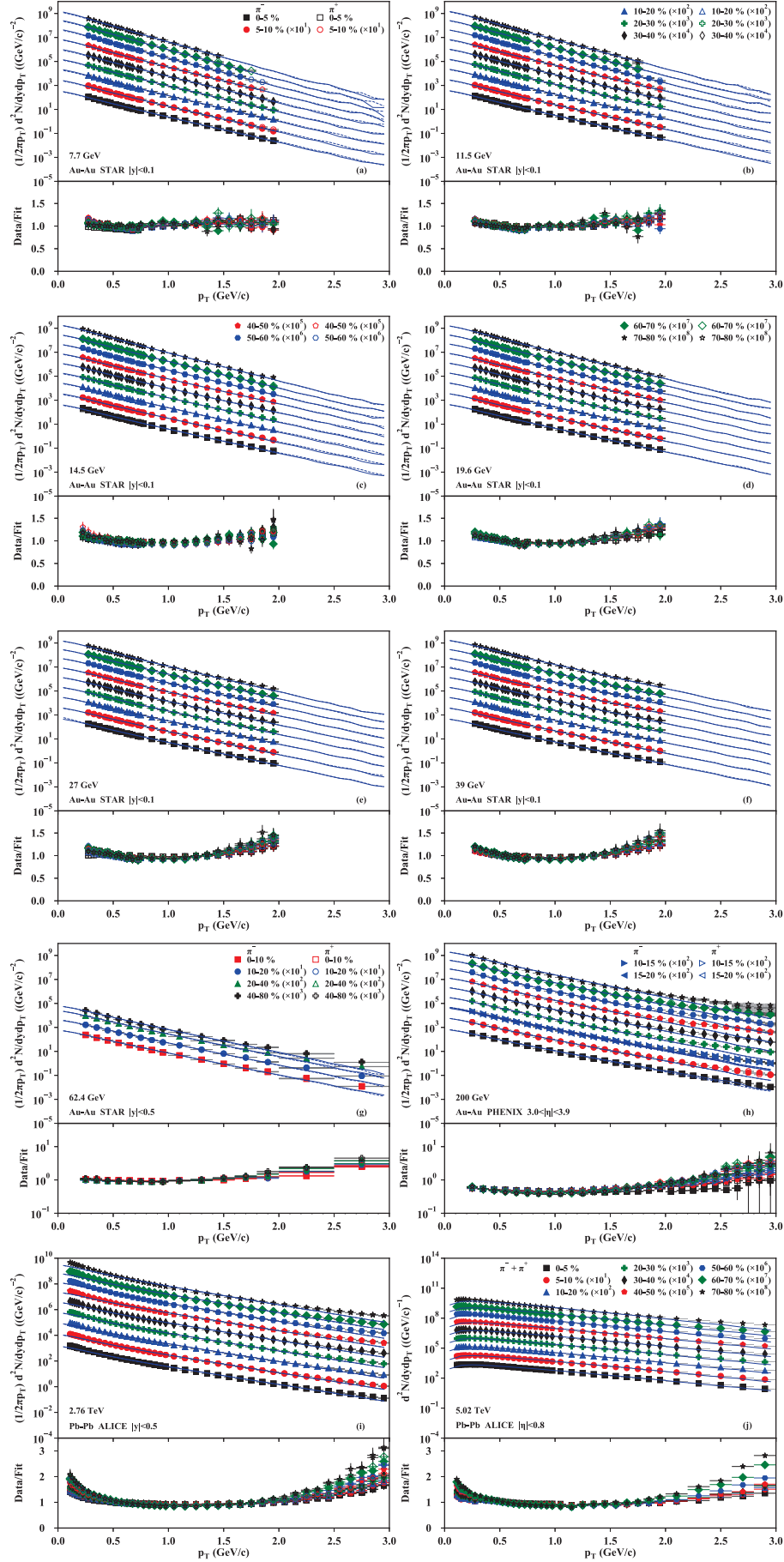


Figure 1. Transverse momentum spectra of π^- and π^+ produced in Au–Au collisions at $\sqrt{s_{NN}} = 7.7$ GeV (a), 11.5 GeV (b), 14.5 GeV (c), 19.6 GeV (d), 27 GeV (e), 39 GeV (f), 62.4 GeV (g), and 200 GeV (h), as well as in Pb–Pb collisions at 2.76 TeV (i) and 5.02 TeV (j) with various centrality classes and given mid-rapidity. The symbols represent the experimental data measured by the STAR [30–34] and ALICE [35, 36] Collaborations and re-scaled by different amounts marked in the panels. The curves are our results fitted by the Bose-Einstein distribution with embedded transverse expansion velocity.

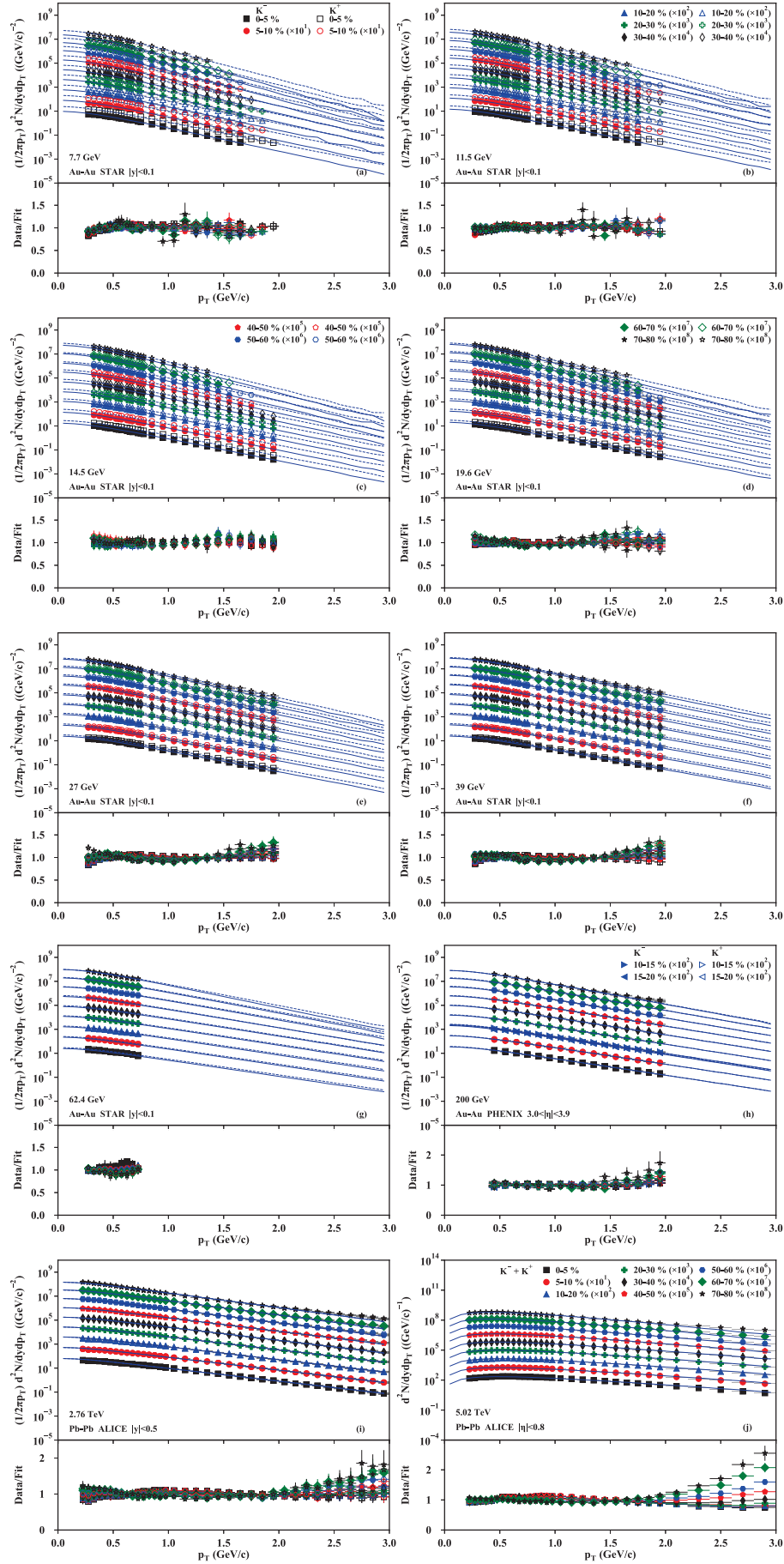


Figure 2. Same as Figure 1, but showing the transverse momentum spectra of K^- and K^+ . The curves are our results fitted by the Bose-Einstein distribution with embedded transverse expansion velocity.

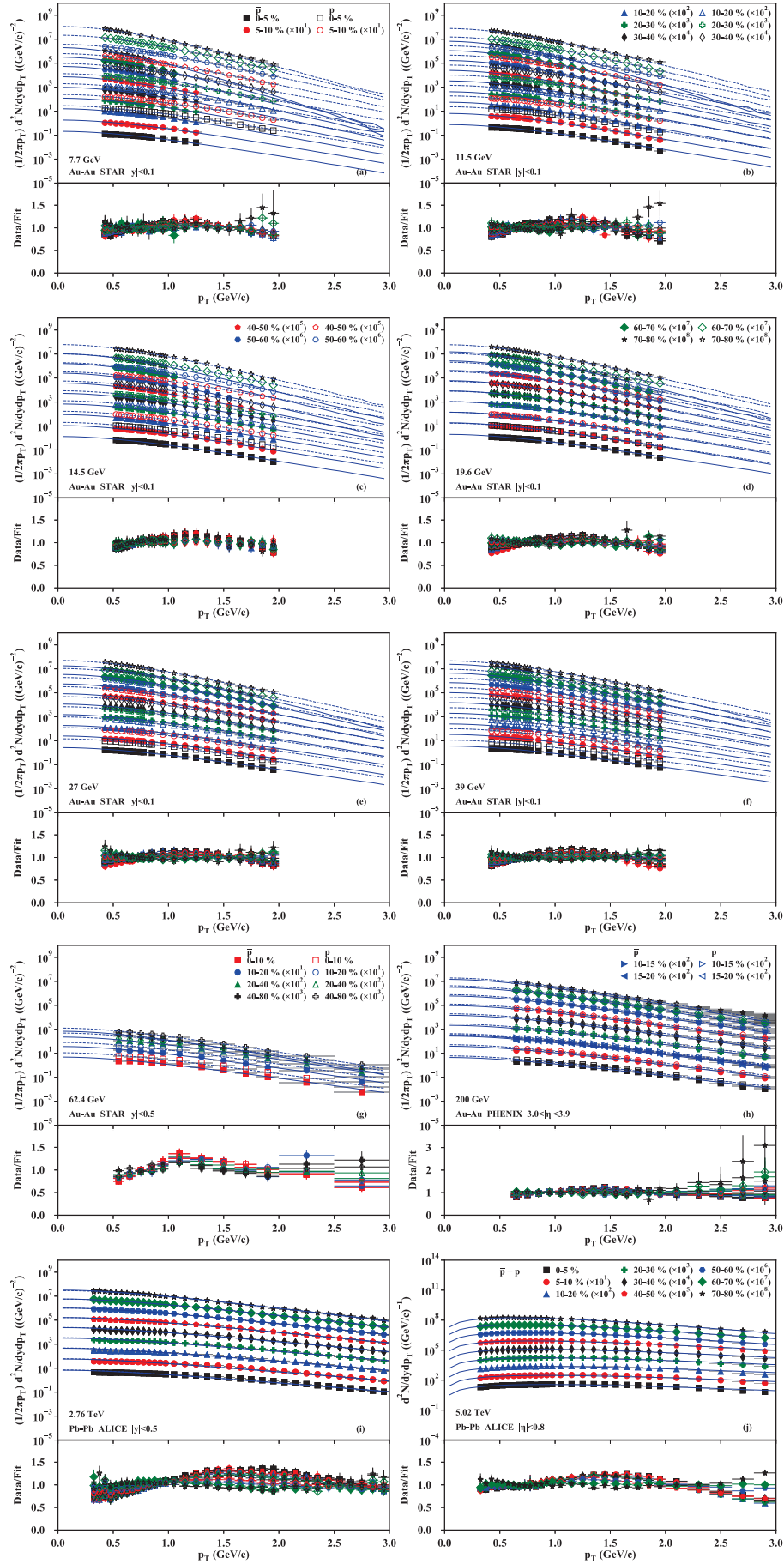


Figure 3. Same as Figure 1, but showing the transverse momentum spectra of \bar{p} and p . The curves are our results fitted by the Fermi-Dirac distribution with embedded transverse expansion velocity.

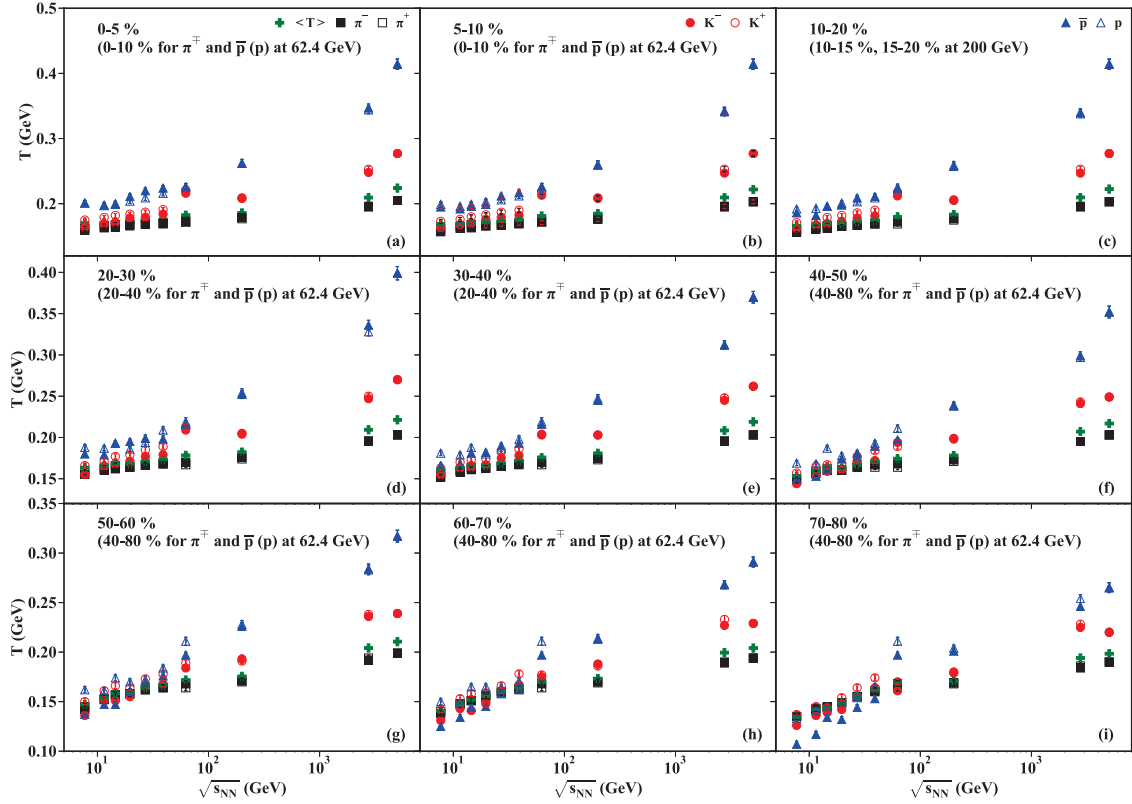


Figure 4. Dependence of the kinetic freeze-out temperature T on the collision energy $\sqrt{s_{NN}}$, centrality, and particle mass or type. From panels (a) to (i), the centrality classes are mainly 0–5%, 5–10%, ..., and 70–80%, respectively. The closed (open) squares, circles, and triangles represent the results for π^- (π^+), K^- (K^+), and \bar{p} (p), respectively, where the closed symbols at 5.02 TeV are not undistinguished the charges. The crosses represent the average T ($\langle T \rangle$) weighted over the yields of different particles. All symbols represent the results fitted from Figures 1–3.

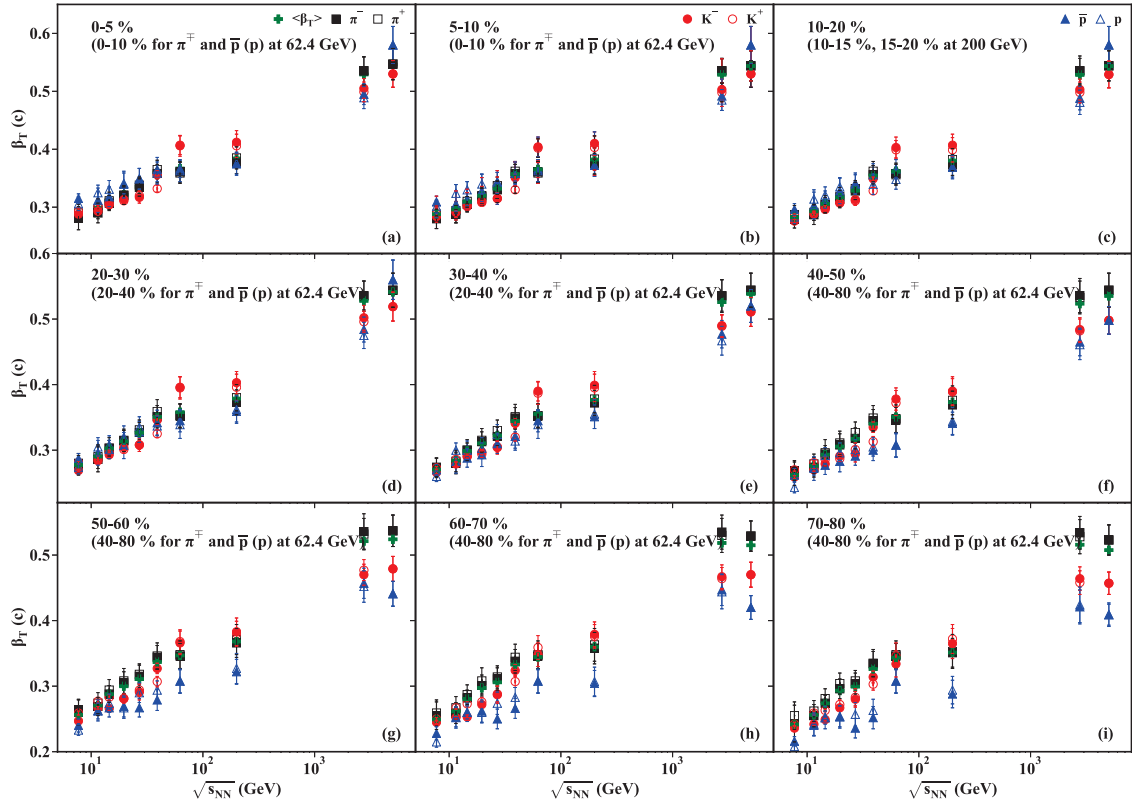


Figure 5. Same as Figure 4, but showing the dependence of the transverse expansion velocity β_T on the collision energy $\sqrt{s_{NN}}$, centrality, and particle mass. The average β_T ($\langle \beta_T \rangle$) is the weighted average over the yields of different particles.